Deformation-Induced Conformational Changes in Stretched Samples of Amorphous Poly(ethylene terephthalate)

J. C. RODRÍGUEZ-CABELLO, J. C. MERINO, L. QUINTANILLA, and J. M. PASTOR*

Dpt. Física de la Materia Condensada, Facultad de Ciencias/E.T.S.I.I., Universidad de Valladolid, Spain

SYNOPSIS

The combination of Fourier transform Raman spectroscopy and thermal analysis has been proved to be adequate for the study of the quantitative structural changes which take place in amorphous poly(ethylene terephthalate) on stretching. The two-phase conformational model previously proposed for annealed samples was applied to uniaxially stretched samples. The samples were deformed at different temperatures and speeds. Different conformer contents were found in the stretched sample depending on the stretching conditions. In general, deformation induces a conformational transition of *gauche* to *trans*. This behavior was lost at a narrow range of temperatures above the glass transition and at the lowest speeds, where the stretching seemed not to induce conformational changes. This different behavior has been associated to the high mobility of the polymer chains under these conditions, which imposes a different process of deformation marked by a high degree of chain slipping. This kind of deformation is present all along the sample and with the absence of necking in the uniaxial drawing process. © 1996 John Wiley & Sons, Inc.

INTRODUCTION

Vibrational spectroscopy has become one of the most important tools for the characterization of the chemical and physical nature of polymers. In principle, the complementary techniques of infrared and Raman spectroscopy provide qualitative and quantitative information about structural details of the polymer under examination such as nature and composition, steric and conformational order, three-dimensional state of order, and orientation.[1-5]

The need for structural analysis of samples requires the use of nondestructive sampling procedures which allow analysis of the specimen with minimum sample preparation. In the last decade, the well-deserved reputation of FTIR[6-9] has generated hopes for similar benefits in Raman spectroscopy. Despite the major experimental difficulties with FT–Raman spectroscopy, the recent development of this technique in the near-infrared region allows one to obtain spectra with an SNR similar to that in the best conventional Raman instruments. Moreover, the problem of fluorescence has been reduced because of working in the near-infrared.[3,10-13]

Vibrational spectra of PET have been studied in detail.[14-28] The PET Raman bands are assigned to different parts of the polymer: the benzene ring and glycol residue. The conformational sensitive bands are also known. In the crystalline state, PET is present in an almost planar form according to X-ray diffraction analysis, and the ethylene glycol fragment has a *trans* structure. In the amorphous state, PET has a more complicated conformational composition and both *trans* and *gauche* conformations of the above segment can be present.[14,15]

In spite of the importance of vibrational spectroscopy for the characterization of macromolecular structure, only a limited number of problems may be solved by its exclusive application. A more complete picture of polymer structure can be obtained by an appropriate choice and combination of different methods. In this particular case, although PET is a semicrystalline polymer, the spectral features of the *trans* isomer in the crystalline and disordered phases must be similar as they are not resolved under these experimental conditions.[17] Then, in this work,

* To whom correspondence should be addressed.

Journal of Applied Polymer Science, Vol. 62, 1953–1964 (1996)
 CCC 0021-8995/96/111953-12

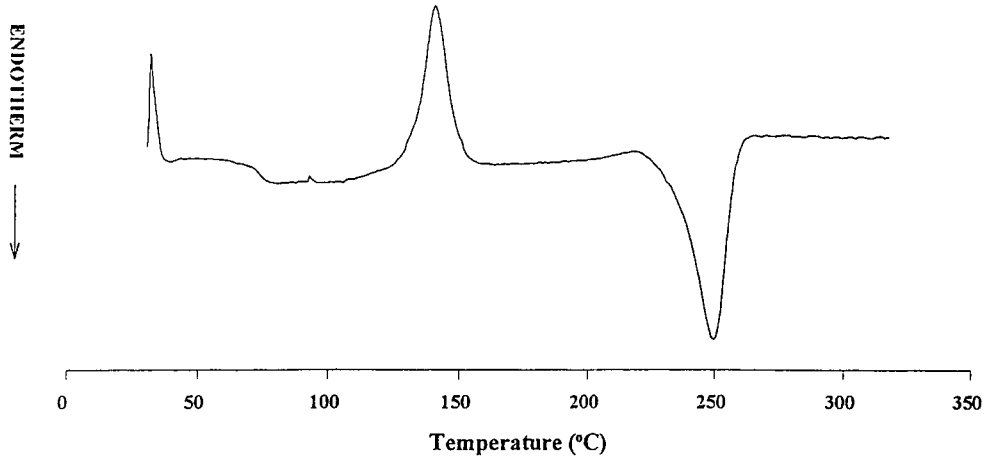

Figure 1 Typical thermogram of the amorphous PET samples used in this work.

differential scanning calorimetric (DSC) measurements were correlated with FT–Raman spectroscopy in order to quantify the distribution of the *trans* isomer in the ordered and disordered regions of the deformed PET samples.

In a previous article, and by combining these two techniques, we reported the changes in the isomer content of semicrystalline PET samples subjected to different thermal treatments.[29] The present article was intended to extend those results by studying the changes in the conformational contents of amorphous PET samples uniaxially deformed at different stretching temperatures and speeds.

EXPERIMENTAL

Materials

PET pellets (Polyclear T 86 [78]) were kindly supplied by Hoechst (Portalegre, Spain). The pellets were molded in a hot press to obtain 1 mm-thick plates. The pellets were heated up to 300°C for 10 min and then the mold with the molten material was rapidly quenched in liquid nitrogen. By these means, PET plates with a very low degree of crystallinity were obtained (see Fig. 1 for a typical thermogram and Fig. 2 for the Raman spectra of the unstretched PET sample). The samples were cut from the 1 mm-thick plates by a die into the conventional dumbbell shape for the stretching test (type III, norm ASTM D 638-77).

Stretching of the Samples

The specimens were uniaxially stretched with an universal testing machine (Instron, Model 6025) provided with a thermostatic chamber which allows stretching processes at temperatures above room temperature. The speeds tested were 0.1, 1, 10, 100, and 1000 mm/min, and for each speed, stretching at 23 (room temperature), 50, 70, 90, 130, 170, and 200°C was done. The samples were maintained in the hot chamber for 30 s before stretching. The stretching was carried out until a deformation of 100% was achieved and the sample was immediately quenched to room temperature. The stress–strain curves obtained for the speed of 0.1 mm/min are shown in Figure 3 as an example of the mechanical behavior. Some differences were found in the stretching behavior at the different temperatures and speeds, which will be further discussed, but some of the stretching conditions led to the formation of a clear neck and others did not. All samples were stretched to 100% strain, but this must not be understood as true strain because this will strongly depend on the deformation characteristics of the particular sample. However, since true strains will not play a significant role in our discussion, this value is not included.

Fourier Transform Raman Measurements

The Raman instrument was a Bomem Series MB 155 consisting of an FT–Raman compartment attached to the Michelson MB 155 FTIR spectrometer, thus allowing both FT–Raman and FTIR analyses to be made. Excitation for FT–Raman experiments was obtained with a near-infrared diode-pumped solid-state Nd^{3+} : YAG laser operating at 1.06 μm. The laser used here, a laser Diode-LDP 1000 series, provides up to 2 W of power (TEM_{00}). Plasma filters were placed on the output

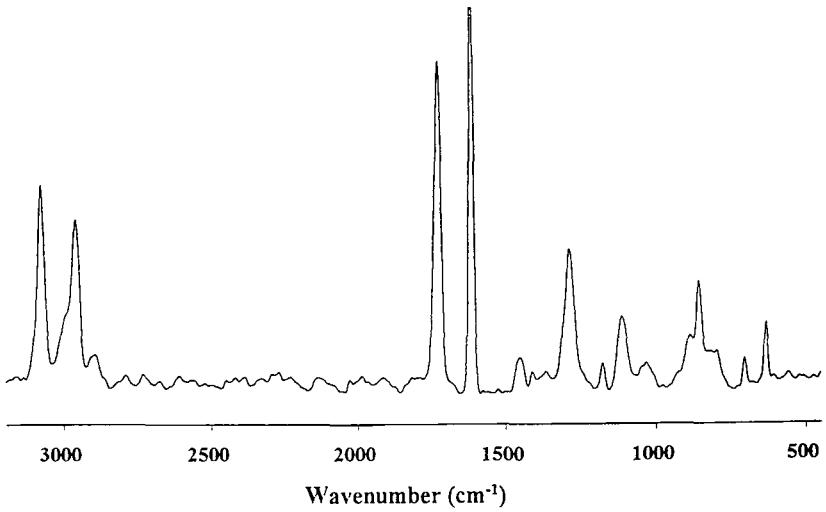

Figure 2 FT-Raman spectra of the amorphous PET samples.

of the laser to eliminate the plasma lines emitted by the laser. In the macroconfiguration, a beam of approximately 2 mm diameter was focused by a lens situated just after the plasma filter onto the sample. The spot size obtained at the sample was of the order of 200 μm. The backscattered light was collected by an ellipsoidal mirror and directed to the interferometer and finally detected by an InGaAs detector, cooled thermoelectrically. Another small mirror can be put in the path of the scatter beam after the collecting mirror to deflect some of the radiation to a CCD video camera that permits simultaneous visualization of the sample and the laser spot. Two dielectric filters were used to cut off intense laser reflections and the Rayleigh radiation. The combination of high-rejection laser filters and the cooled InGaAs detector allowed Raman spectra in the range 200–3350 cm^{-1} to be obtained. A He—Ne rejection filter was also positioned in the IR sample compartment to keep radiation from the He—Ne laser of the interferometer from reaching the detector. Spectra were recorded at 4 cm^{-1} resolution and averaged over 750 scans with a laser power of 1 W. The spectra illustrated here were not corrected for instrumental response.

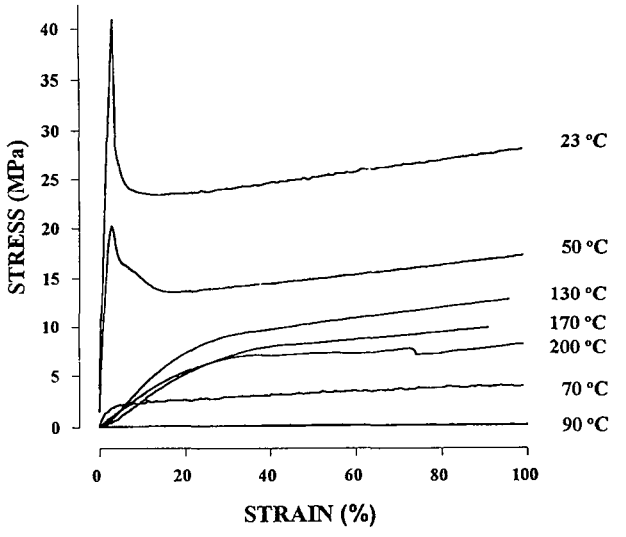

Figure 3 Stress–strain curves for the stretched PET samples (stretching speed 0.1 mm/min).

One fundamental problem in quantitative Raman analysis for this kind of experience is anisotropy because changes in the intensity of one particular Raman band could be due to the changing nature of the anisotropy rather than to a change in the number of Raman species. To avoid artifacts coming from the anisotropy of the studied samples, neither polarizers nor analyzers were placed on the incident and scattered beams. Furthermore, since some of the studied samples can show a high degree of chain orientation, a depolarizer (CVI DPL-10-1060) was placed between the plasma filters and the focusing lens to avoid artifacts coming from the inherent polarization of the incident laser. To test the method's validity, Raman spectra of a highly deformed PET sample were obtained for different orientations of the sample which ranged between completely vertical in the sample chamber to horizontal. The obtained spectra did not show significant differences (result not shown). Thus, with this setup, changes in intensity of the Raman bands cannot be attributed to anisotropy of the samples.

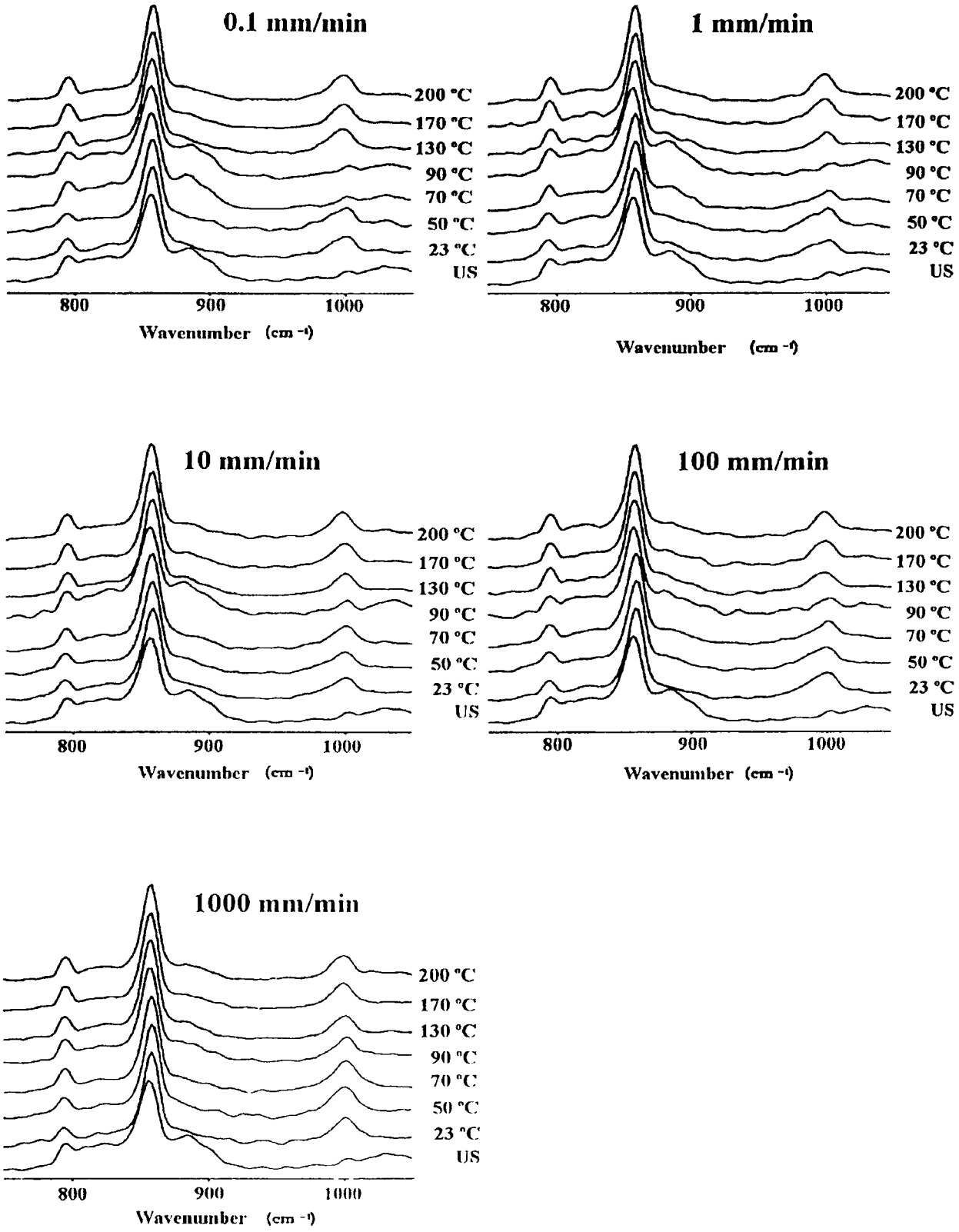

Figure 4 FT–Raman spectra of the deformed PET samples. US: undeformed sample.

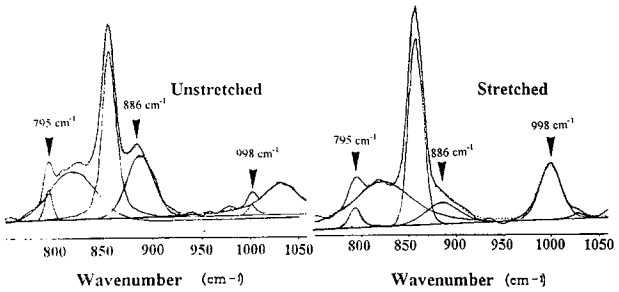

Figure 5 FT-Raman spectra in the selected wavenumber range of an unstretched and a stretched PET sample. Solid line: Original spectra and different band contributions. Dotted line: Addition of the different contributions.

Differential Scanning Calorimetric Measurements

Thermal analysis were carried out in air with PET specimens whose weight ranged between 5 and 7 mg. The DSC experiments were performed on a Mettler TA 4000 (DSC 30) instrument at a heating rate of 10°C min^{-1}; each thermogram was recorded from 25 to 320°C. The calibration of both temperature and melting enthalpy was made with a standard sample of indium.

From the measured heat of fusion, ΔH_{exp}, an apparent degree of crystallinity, $\%C_{DSC}$, was determined according to the equation

$$\%C_{DSC} = \frac{\Delta H_{exp}}{\Delta H^0} \cdot 100 \qquad (1)$$

where ΔH^0 is the heat of fusion of an ideal PET crystal for which we adopted the value of 28.1 cal g^{-1} (1 cal = 4.184 J).[30] Finally, since amorphous or low-crystallinity PET samples crystallize in the DSC during the time it takes to heat from the glass transition temperature to the melting point, the area of the melting peak includes the contribution from these newly formed crystals. However, in this case, an exothermic peak coming from the crystallization process can be observed on the thermogram and its integral, following the conventional method used for this kind of polymer, can be substracted from the final melting peak to obtain the original crystallinity value.

RESULTS AND DISCUSSION

Vibrational Analysis

In the Raman spectra of PET, bands adequate to study the isomer content[29] fall in the range between 750 and 1050 cm^{-1}. The band situated at 998 cm^{-1} (O — CH_2 stretching of the *trans* isomer[16]) and that at 886 cm^{-1} (assigned to a *gauche* conformation in the ethylene glycol segments[25]) are the bands analyzed in this work. The selected range FT-Raman spectra of the stretched PET samples are shown in Figure 4. By a first inspection of this figure, some results can be advanced: The unstretched samples (US on the figure) showed high values of the band related to the *gauche* isomer (886 cm^{-1}) denoting a high percentage of this isomer. On the contrary, the Raman spectra of the stretched samples showed a high increase of the band associated to the *trans* isomer (998 cm^{-1}) and a complementary decrease of the intensity of the band at 886 cm^{-1} at all stretching temperatures except at the lowest stretching speeds for the temperatures of 70 and 90°C. Then, the stretching of the PET amorphous samples promotes a clear shift in the isomer content. The spectra of the stretched material in those conditions is similar to the unstretched samples, so we can assume that the isomer content was not greatly modified. In the next experiments (DSC), we will quantify the isomer distribution in the ordered and disordered zones and its correlation with the different stretching conditions. Also, a different state of disorder in the amorphous regions will be proposed by the quantification of its isomer distribution. Finally, we will also justify the peculiar spectroscopic and calorimetric behavior observed at 70 and 90°C.

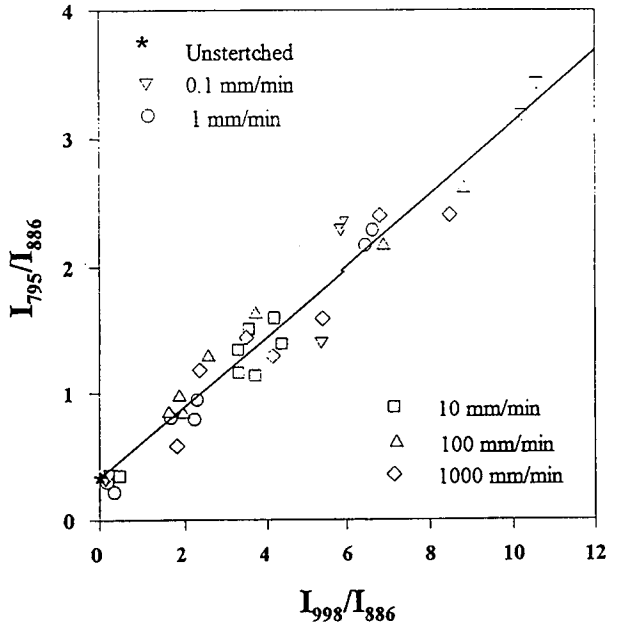

Figure 6 Least-square fitting of the experimental data to the two-phase conformational model.

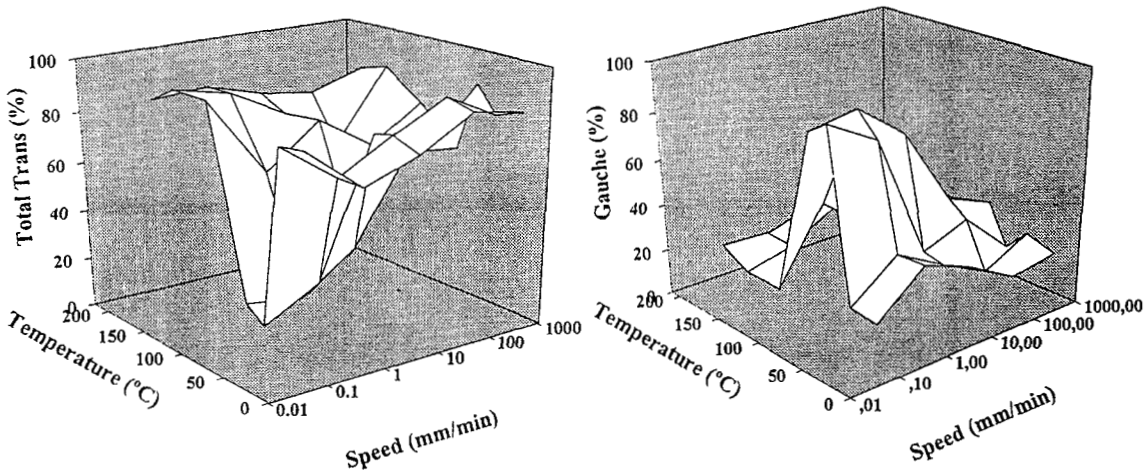

Figure 7 *Trans* and *gauche* isomer contents vs. stretching speed and temperature.

Quantitative Analysis

In Raman spectroscopy, the value resulting from the integration of spectral bands are often used for quantitative analysis. However, in the spectral range where the bands of interest appear, there are other bands which make their direct integration difficult. So, a method of band deconvolution and peak fit has to be used here. The method is based on the Marquardt–Levenberg algorithm for nonlineal regression. The Raman bands were fit to the conventional Lorentzian–Gaussian profile. We considered six bands in the range of 750–1050 cm^{-1}. All parameters were set free during the fitting process to avoid subjective interferences by the operator; an example of the performance of the band separation can be seen in Figure 5. Following these calculations, the Raman I_{988}/I_{795} and I_{886}/I_{795} were calculated; the integral intensity of the band at 795 cm^{-1} was used as the internal reference band.

Since only two conformational isomers are possible in PET samples and, in the case of *trans,* its presence in amorphous or ordered phases is not reflected by any spectroscopical feature, PET could be considered to satisfy a two-phase conformational model similar to the model proposed elsewhere[9,29] on annealed PET samples in the infrared and Raman domains. For the Raman bands, the following relationship should hold:

$$p_1\left(\frac{I_{998}}{I_{795}}\right) + p_2\left(\frac{I_{886}}{I_{795}}\right) = 1 \qquad (2)$$

where p_1 and p_2 are the 998 and 886 cm^{-1} band weights, respectively. This equation can be written as

$$\frac{I_{795}}{I_{886}} = p_1\left(\frac{I_{998}}{I_{886}}\right) + p_2 \qquad (3)$$

and the representation of this equation for the samples at the experimental processes is shown in Figure 6. The good correlation found in the least-squares fitting reveals the adequacy of the model. The values of p_1 and p_2 can be obtained from that fitting (p_1 = 0.279, p_2 = 0.330, coefficient of linear regression CLR = 0.988). The individual isomer distribution at the different stretching conditions, as calculated from $p_1(I_{998}/I_{795})$ and $p_2(I_{886}/I_{795})$, can be observed in Figure 7; the isomer distribution of the unstretched samples was about 78% of the *gauche* isomer and 20% of the *trans* with an estimated error below 5%.

The samples stretched at temperatures out of the range 70–90°C tended to show similar isomer distribution independently of the stretching speed. Then, in spite of the differences in stretching conditions, samples with no significant differences in the isomer contents were finally obtained. As was previously advanced, that general trend was not fulfilled at the temperatures of 70–90°C. Furthermore, in contrast to the lack of a clear influence of the stretching speed found for the rest of temperatures tested, in the range 70–90°C, the influence of the kinetics of the process is clear. At the lowest speeds, the isomer content is similar to the one found on the unstretched samples. As the speed increases, the isomer content is progressively changing until, at the highest speeds, the percentages of *trans* and *gauche* are similar to the ones found at the other temperatures.

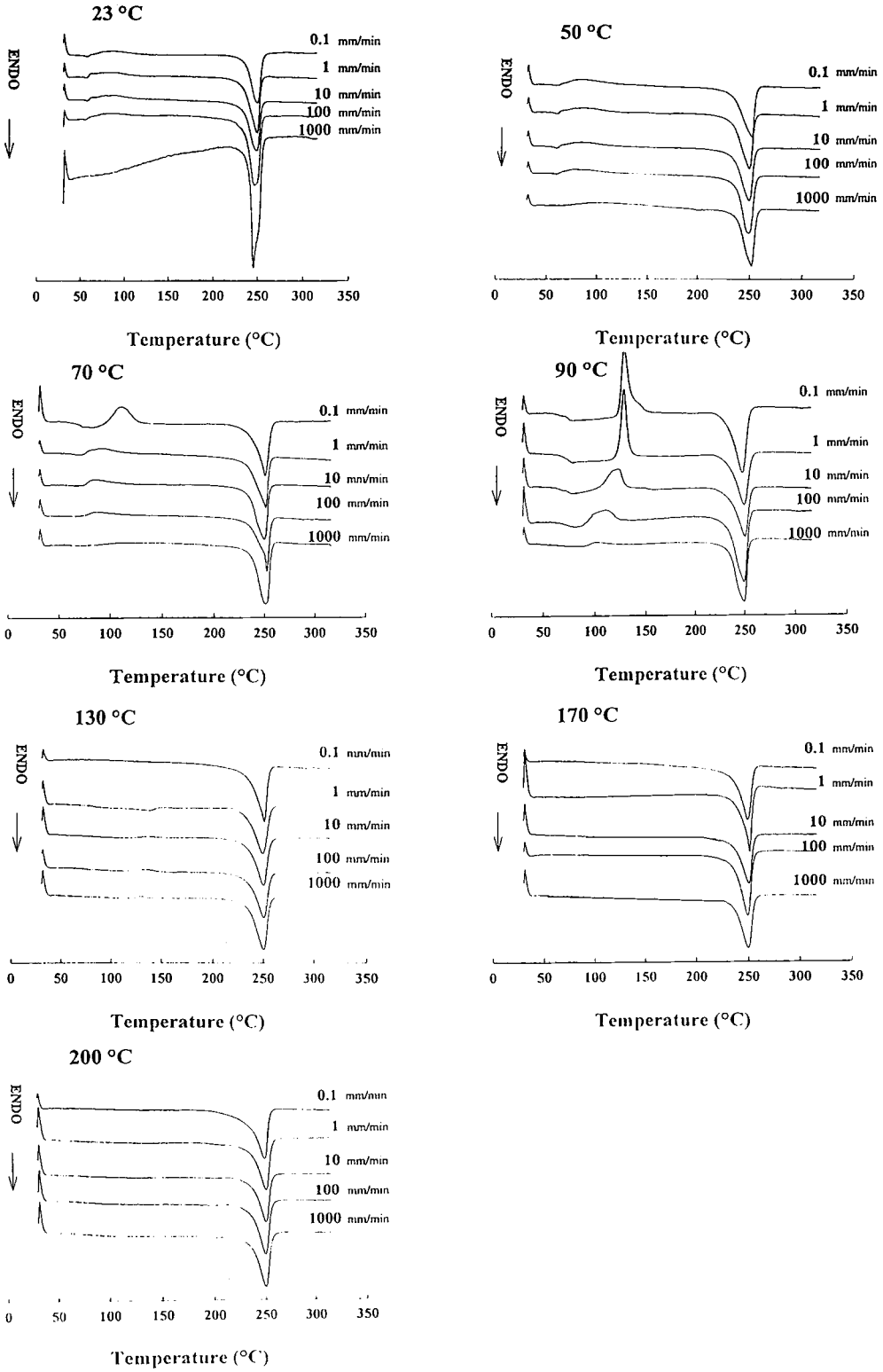

Figure 8 Thermograms of the deformed PET samples.

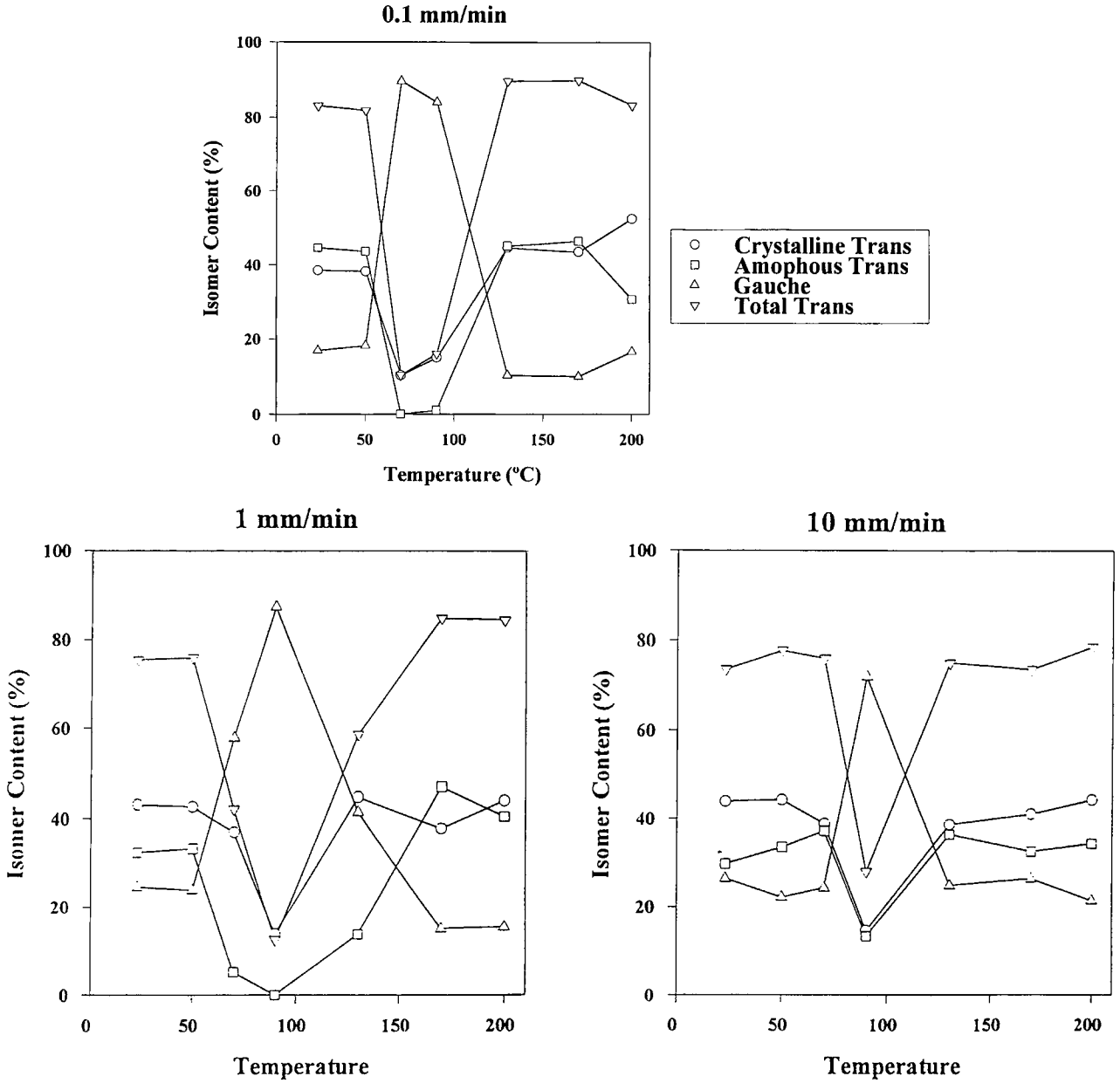

Figure 9 Isomer distribution vs. stretching speed and temperature for the deformed PET.

The study of the chain structure in the amorphous zones in both "normal" and abnormal stretching processes needs the quantitative analysis of the evolution of the *trans* isomer in the crystalline and disordered phases. For that purpose, we used differential scanning calorimetry (DSC) estimations of the crystallinity of the stretched samples. In this way, the percentage of crystallinity can be assumed as the percentage of *trans* in the ordered phase, since only this isomer can exist in those zones. The content of the *trans* isomer in the amorphous zones can be estimated by the difference of the total *trans*, spectroscopically obtained, and the DSC value.

Thermal Analysis and Complete Conformational Distribution

We used for this work the thermal analysis reported previously.[9,29] DSC thermograms of stretched PET are shown in Figure 8. The deflection of the base

line related to the glass transition can be clearly detected only for samples stretched at 70–90°C, especially at the lowest stretching speeds. For other temperatures, this transition is barely perceptible. An exothermic peak can also be observed at those stretching conditions; that peak is attributed to a crystallization process occurring during the DSC run.

The *trans* isomer content provided by the Raman measurements should be higher than the apparent degree of crystallinity obtained by the DSC method because in the Raman contributions the amorphous phase is present, whereas in the latter, only the crystalline regions contribute. This is the observed behavior, and from the estimated crystallinity, all the isomer contributions can be calculated. Those results are plotted in Figure 9.

For temperatures other than 70 and 90°C, the values of crystallinity of the deformed samples are around 40%, whereas the total *trans* percentage is about 80%. That indicates a percentage of about 40% of amorphous *trans*. Then, the most evident effect of the stretching of amorphous PET samples is a *gauche* → *trans* transition which inverts the isomer contents. That transition is accompanied with a stretch-induced crystallization. This general trend seems to be, in the experimental conditions tested here, almost independent of the temperature or speed of stretching. This behavior has an important exception at the temperatures of 70–90°C and low stretching speeds. At 70–90°C, the isomer contents and crystallinity values are similar to the unstretched amorphous samples. In those samples which showed significant changes in the isomer distribution, a first result deserves to be pointed up: The isomer distribution in the amorphous zones drastically changes compared to the original sample (see Table I). There is a comparatively high content of the *trans* isomer, which indicates that the stretching process promotes partial uncoiling of the polymer chains in the amorphous zones, decreasing their entropy and, in consequence, raising the local state of order in the amorphous zones. This ordering is not detectable by DSC, and taking into account the uncoiling and aligning of the chains, this has to be considered as the, at least partial, establishment of a state similar to the one recently proposed in the

Table I Approximate Isomer Content of the Amorphous Regions of Stretched and Unstretched PET Samples

Sample	*Trans* (%)	*Gauche* (%)	*Trans/Gauche*
Unstretched	10	80	0.125
Stretched	40	20	2

The values represent the general trend when the stretching temperatures fall out the range 70–90°C.

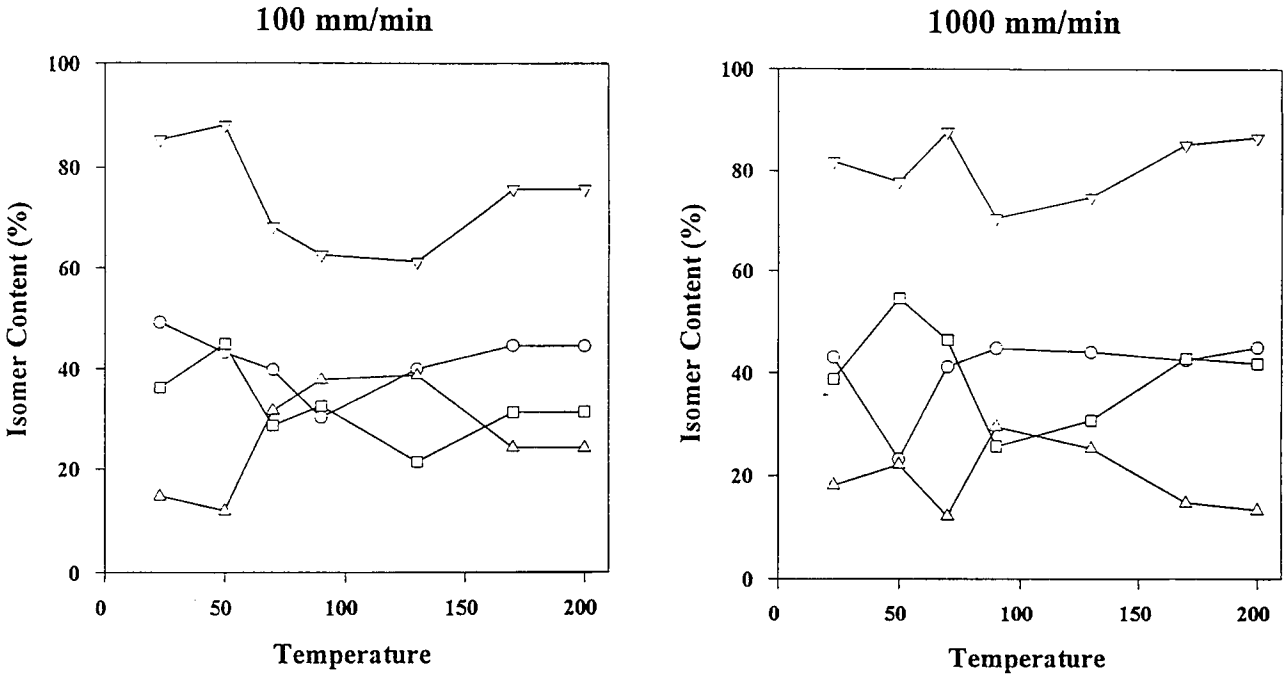

Figure 9 *(Continued from the previous page)*

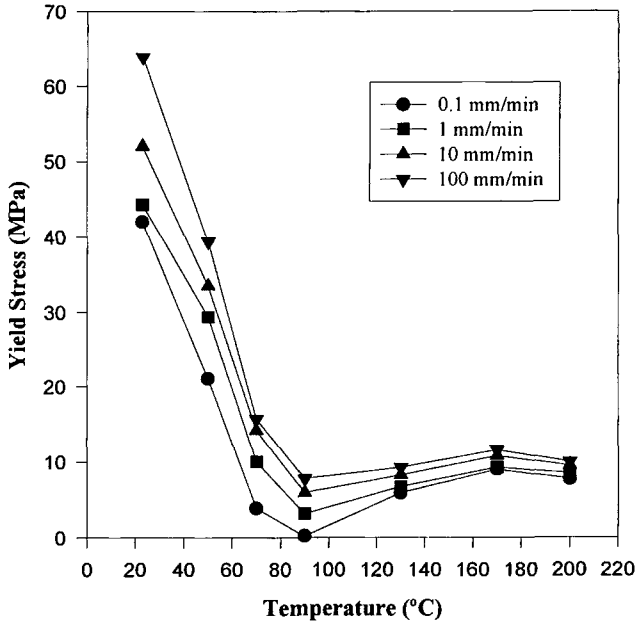

Figure 10 Yield stress vs. stretching speed and temperature.

literature for differents kinds of deformed PET by means of X-ray and density analysis[31,32]: a paracrystalline or distorted crystal structure which is an oriented structure with compact packing of the chains but poor longitudinal and transverse order.

The different isomer distributions observed in the stretched samples is paralleled by the macroscopical behavior. This is evident by observing Figure 10, in which values of the yield stress are plotted vs. stretching speed and temperature. A second macroscopical fact in which this parallelism can be found is neck formation. In this way, the stretching process produced the formation of a neck (and high values of the yield stress) in all the samples which showed significant conformational transitions, being absent (and showing a dramatic drop of yield stress) in those in which the stretching process yielded poor changes of the original isomer contents.

Then, the connection between macroscopical and molecular behavior seems to be the transference of load to the chain which exists during the transformation in the transition front from an isotropous to an oriented material. When the samples deform with formation of a neck, along with an increase of the crystalline content, a high rate of chain orientation is achieved in the stress direction. If the applied load is high enough, conformational transitions are produced from the "coiled" *gauche* chain to the "extended" *trans*.

On the contrary, at temperatures around 70–90°C, the polymer shows a different mechanical behavior. That difference is caused by the proximity of the glass transition (T_g) which occurs in that temperature range (see Figs. 1 and 8). When an amorphous polymer is stretched at its T_g or above, the macroscopical deformation is caused by chain slipping produced all along the sample; this different mechanism is caused by the marked increase in chain mobility.[33]

However, to understand the loss of this behavior and the recovery of a deformation mechanism based on neck formation at temperatures above 90–130°C, we have to keep in mind that this polymer is amorphous only because of the way it was obtained and will suffer a crystallization process when heated at temperatures some degrees above its T_g. Under these conditions, thermal energy is enough by itself to produce conformational changes and crystallization. Furthermore, if this thermal crystallization of PET occurs in stretching operations, it is always much faster than is crystallization under stress-free (undrawn) conditions.[34] In these conditions, we have a semicrystalline material almost from the beginning of the stretching process. Then, the gained mobility of the polymer chains at temperatures above the T_g is rapidly lost by crystallization. The response of semicrystalline polymers to an applied stress, as described by the different deformation models,[35–37] promotes the appearance of a neck.

This explanation is also consistent with the behavior observed at temperatures of 70–90°C at the highest stretching speeds. It is evident that the mobility of the chains strongly depends on the dynamics of the process. When the speed of stretching is high, the mobility of the chains would not be enough and the deformation process, especially at the intermediate speeds tested here, shows a mixture of a process of deformation extended along the whole sample by means of chain slipping and a localized deformation. The visual inspection of the sample reveals the existence of a weak neck. As the speed increases, the predominant process is this last one; the neck became more apparent and the values of crystallinity and isomer distribution close to that observed for other temperatures, where the mobility of the chains are strongly impeded.

CONCLUSIONS

The amorphous PET samples studied here showed a high contribution of the *gauche* isomer (79%) of

the ethylene glycol fragment; the *trans* isomer is present in a percentage about 21%. The stretching of this kind of sample promotes a considerable increase of the crystalline content. These changes are accompanied by significant variations of the conformer content in the amorphous zones. In these, the increase of the *trans* content at the expense of the *gauche* along with the well-known chain orientation has to be understood as a partial ordering of the amorphous regions. This ordering has not been considered as a long-range order since is not detectable by DSC. Furthermore, the final crystallinity and the isomer distributions are almost independent of the stretching conditions. Only a narrow range of temperatures and speeds showed a distinctive behavior (70–90°C and low speeds). This can be interpreted from the point of view of the different mechanical and macroscopical behavior of the deforming samples. Under these special conditions, the stretching results in low values of the stress and without formation of a neck. In that range, temperature is above T_g and polymer chains have high mobility due an increase of their free volume and their consequent weak interchain interaction. The applied stress promotes chain slipping all over the sample which is not hindered by the weak interchain interactions. Under these circumstances, there are low levels of stress and, furthermore, a poor transference of the load to the polymer backbone. The stress on the chain would not be enough to surpass the conformational barriers, being difficult in the presence of significant amounts of *gauche* → *trans* transition. Of these temperatures of stretching, the chain mobility is not high enough and the deformation occurs in localized zones where all the deformation concentrates (the neck). In this case, higher stress levels are achieved with a higher transference of load through the chain backbone which, finally, causes radical changes in the isomer distribution and a considerable increase of the crystallinity. When the temperature is in the 70–90°C range but the stretching speed is high, the mobility of the chains could be, in general, not enough. Under these circumstances, the deformation process would be reasonably described as a mixture of the two processes previously pointed out which yields a conformational distribution which takes intermediate values of the isomer contents. As the speed increases, the last mechanism dominates until, finally, at 100 and 1000 mm/min, the isomer distribution is not significantly different from that obtained at other stretching temperatures.

This research was funded by the Comisión Interministerial de Ciencia y Tecnología (CICYT) (Programme MAT90-914).

REFERENCES

1. R. I. Grose, S. Hvilsted, and H. W. Siesler, *Makromol. Chem. Macromol. Symp.*, **52,** 175 (1991).
2. H. W. Siesler and K. Holland-Moritz, *Infrared and Raman Spectroscopy of Polymers,* Marcel Dekker, New York, 1980.
3. T. Hirschfeld and B. Chase, *Appl. Spectrosc.*, **40,** 133 (1986).
4. P. R. Griffiths and J. A. Haseth, *Fourier Transform Infrared Spectroscopy,* Wiley, New York, 1986.
5. D. W. Green and G. T. Reedy, in *Fourier Transform Infrared Spectroscopy: Application to Chemical Systems,* Ferraro and Basile, Eds., Academic Press, New York, 1985, Vol. 4 p. 1.
6. P. R. Griffiths and M. P. Fuller, *Adv. Infrar. Raman Spectrosc.*, **9,** 63 (1982).
7. J. M. Chalmers and M. W. Mackenzie, *Advances in Applied Fourier Transform Infrared Spectroscopy,* Wiley, Chichester, 1988, p. 105.
8. M. W. Urban and J. L. Köenig, in *Vibrational Spectrum and Structure,* During, Ed., Elsevier, Amsterdam, 1989, Vol. 18, p. 128.
9. L. Quintanilla, J. C. Rodríguez-Cabello, T. Jawhari, and J. M. Pastor, *Polymer,* **34**(18), 3787 (1993).
10. B. Chase, *Anal. Chem.*, **59,** 881A (1987).
11. B. Chase, *Mikrochim. Acta.*, **3,** 81 (1987).
12. P. Hendra, C. Jones, and G. Warnes, *Fourier Transform Raman Spectroscopy,* Ellis Horwood, Chichester, 1991.
13. Rabolt et al., *Appl. Spectrosc.*, **41,** 721 (1987).
14. I. M. Ward and M. A. Wilding, *Polymer,* **18,** 327 (1977).
15. A. J. Miyake, *Polym. Sci.*, **38,** 479 (1959).
16. F. J. Boerio and K. Bahl, *J. Polym. Sci. Polym. Phys. Ed.*, **14,** 1029 (1976).
17. S. B. Lin and J. L. Köenig, *J. Polym. Sci. Polym. Phys. Ed.*, **21,** 2277 (1983).
18. S. S. Sheiko, I. S. Viainilovitch, and S. N. Magonov, *Polym. Bull.*, **25,** 499 (1991).
19. M. Yazdanian, I. M. Ward, and H. Brody, *Polymer,* **26,** 1779 (1985).
20. L. d'Esposito and J. L. Köenig, *J. Polym. Sci. Polym. Phys. Ed.*, **14,** 1731 (1976).
21. X. Yang, F. Long, D. Shan, and R. Quian, *Polym. Commun.*, **32,** 125 (1991).
22. H. M. Heuvel and R. Huisman, *J. Appl. Polym. Sci.*, **30,** 3069 (1985).
23. S. B. Lin and J. L. Köenig, *J. Polym. Sci. Polym. Phys. Ed.*, **21,** 2365 (1983).
24. J. M. Pastor, A. Gonzalez, and J. A. de Saja, *J. Appl. Polym. Sci.*, **38,** 2283 (1989).

25. J. Štokr, B. Schneider, D. Doskočilová, J. Lövy, and P. Sedláček, *Polymer,* **23,** 714 (1982).
26. S. B. Lin and J. L. Köenig, *J. Polym. Sci. Polym. Phys. Ed.,* **21,** 2067 (1983).
27. I. J. Hutchison and I. M. Ward, *Polymer,* **21,** 55 (1980).
28. J. L. Köenig and M. J. Hannon, *Macromol. Sci. Phys. B,* **1,** 119 (1967).
29. J. C. Rodriguez-Cabello, L. Quintanilla, and J. M. Pastor, *J. Raman Spectrosc.,* **25,** 335 (1994).
30. A. Mehta, U. Gaur, and B. Wunderlich, *J. Polym. Phys. Ed.,* **16,** 289 (1978).
31. V. B. Gupta, J. Radhakrishnan, and S. K. Sett, *Polymer,* **34,** 3814 (1993).
32. V. B. Gupta, J. Radhakrishnan, and S. K. Sett, *Polymer,* **35,** 2560 (1994).
33. T. H. Courtney, *Mechanical Behaviour of Materials,* McGraw-Hill, New York, 1990.
34. G. Le Bourvellec, L. Monerie, and J. P. Jarry, *Polymer,* **28,** 1712 (1987).
35. A. Peterlin, *J. Mater. Sci.,* **6,** 490 (1971).
36. K. Kobayashi, *J. Polym. Sci. A,* **2,** 211 (1975).
37. J. Petermann, W. Kluge, and H. Gleiter, *J. Polym. Sci. Polym. Phys. Ed.,* **17,** 1043 (1979).

Received November 3, 1995
Accepted June 10, 1996